

## Observations of nearshore crescentic sandbars

I. M. J. van Enckevort,<sup>1</sup> B. G. Ruessink,<sup>1</sup> Giovanni Coco,<sup>2,3</sup> K. Suzuki,<sup>4</sup> I. L. Turner,<sup>5</sup> N. G. Plant,<sup>6</sup> and R. A. Holman<sup>7</sup>

Received 19 November 2003; revised 25 March 2004; accepted 5 May 2004; published 29 June 2004.

[1] The temporal and spatial variability of crescentic sandbars is analyzed with hourly long-term (months) video observations collected at four barred sites and are qualitatively compared to the temporal and spatial variability predicted by hypotheses underpinning existing approaches and models for crescentic bar formation (edge-wave template model, linear stability analysis, and nonlinear models). The observations, coming from the single barred beaches at Duck (North Carolina, USA) and Miyazaki (Kyushu, Japan), and from the double-barred beaches at the northern Gold Coast (Queensland, Australia) and Noordwijk (Netherlands), show that crescentic sandbar wavelength and amplitude variations over space and time are very common. For instance, at any moment in time, the wavelength of the smallest and longest crescentic bar can differ by a factor of 2. Temporal changes in wavelength and amplitude result from merging and splitting of individual crescents, causing the “final” configuration of a crescentic sandbar system to be very different from the initial configuration. The Gold Coast data indicate that these intrinsically nonlinear interactions are an attempt of the crescentic bar system to self-organize into a more uniform pattern, as splitting is usually confined to the longest crescentic bar observed, whereas merging usually combines the smallest crescentic bars into a longer bar. The observed spatial and temporal crescentic bar behavior contrasts qualitatively with behavior predicted from the edge-wave template model and implies that the predictive skill of linear stability models is limited. Nonlinear models are potentially better suited for a comparison against these field observations; several suggestions to improve these models, and hence to facilitate a data-model comparison, are made. *INDEX TERMS:* 4546 Oceanography: Physical: Nearshore processes; 3045 Marine Geology and Geophysics: Seafloor morphology and bottom photography; 3020 Marine Geology and Geophysics: Littoral processes; 4275 Oceanography: General: Remote sensing and electromagnetic processes (0689); *KEYWORDS:* nearshore crescentic sandbars

**Citation:** van Enckevort, I. M. J., B. G. Ruessink, G. Coco, K. Suzuki, I. L. Turner, N. G. Plant, and R. A. Holman (2004), Observations of nearshore crescentic sandbars, *J. Geophys. Res.*, 109, C06028, doi:10.1029/2003JC002214.

### 1. Introduction

[2] The surf zone of sandy beaches usually shows a variety of complicated morphological patterns that sometimes exhibit a remarkable alongshore periodicity. Crescen-

tic sandbars, also known as lunate bars [Shepard, 1952], are a well-known example of such rhythmic patterns. They are shaped as crescent moons parallel to the shore and can be viewed as an alongshore sequence of horns (shoals) and bays (cross-shore troughs) alternating shoreward and seaward of a line parallel to the coast. Occasionally, crescentic bars are associated with similar rhythmic protuberances in the shoreline [e.g., Sonu, 1973; Dolan et al., 1974], known as shoreline rhythms, shoreline sandwaves, or megacusps.

[3] Crescentic bars have been found in pocket beaches and along straight sandy coasts on slopes  $\beta$  (of the barred part of the profile) less than 1:20–1:30 in predominantly nontidal to microtidal settings (Table 1). Reported wave lengths  $L$ , defined as the alongshore distance between consecutive horns, vary over two orders of magnitude, from several tens of meters to a few kilometers (Table 1). Usually,  $L$  increases with distance offshore  $D$ , in particular in multiple bar systems, where the outer bar may have length scales an order of magnitude larger than in more shoreward bars [e.g., King and Williams, 1949; Clos-Arceud, 1962a; Sonu, 1973; Barousseau and Saint-Guily, 1981]. There is,

<sup>1</sup>Institute for Marine and Atmospheric Research, Department of Physical Geography, Faculty of Geosciences, Utrecht University, Utrecht, Netherlands.

<sup>2</sup>Complex System Laboratory, Cecil and Ida Green Institute of Geophysics and Planetary Physics, University of California, San Diego, La Jolla, California, USA.

<sup>3</sup>Now at National Institute of Water and Atmospheric Research Ltd., Hamilton, New Zealand.

<sup>4</sup>Marine Environment and Engineering Department, Port and Airport Research Institute, Yokosuka, Japan.

<sup>5</sup>Water Research Laboratory, School of Civil and Environmental Engineering, University of New South Wales, Sydney, Australia.

<sup>6</sup>Naval Research Laboratory, Stennis Space Center, Mississippi, USA.

<sup>7</sup>Coastal Imaging Laboratory, College of Oceanic and Atmospheric Sciences, Oregon State University, Corvallis, Oregon, USA.

**Table 1.** Observations of Crescentic Bars, Ordered by Publication Year

Site	Setting	Tide, m	Slope, 1/β	<i>L</i> , m	<i>A</i> , m	<i>c<sub>m</sub></i> , m/day	Reference
Mediterranean <sup>a</sup>	mainly pocket	≈0	-	-	-	-	<i>King and Williams</i> [1949]
Panama City, FL, USA	straight	-	-	≈300	-	-	<i>Shepard</i> [1952]
Skaw, Denmark	straight (spit)	-	-	200–300	-	-	<i>Bruun</i> [1954]
Côte des Maures, France	pocket	≈0	-	100	-	-	<i>Arbey</i> [1959]
Leucate Beach, France	straight	≈0	-	100–250	-	-	<i>Rivière et al.</i> [1961]
Cape Kalaa and El Madr, Algeria	pocket	≈0	-	500	-	-	<i>Clos-Arceduc</i> [1962b]
They de la Gracieuse, France	straight (spit)	≈0	-	100–120	-	-	<i>Clos-Arceduc</i> [1962a]
Point de l’Espiguette, France	straight	≈0	-	150–180	-	-	<i>Clos-Arceduc</i> [1962a]
Various, Japan	straight	-	>50	40–1000	-	-	<i>Homma and Sonu</i> [1962]
Various, USA	straight (?)	micro	-	≈100–3000	-	-	<i>Sonu</i> [1973]
New Brunswick, Canada	straight	0.4–1.3	200	288–1232	18–68	0.3	<i>Greenwood and Davidson-Arnott</i> [1975]
White Park Bay, Ireland	pocket	1.8	100	105–450	-	-	<i>Carter and Kitcher</i> [1979]
Narrabeen Beach, Australia	pocket	1.3–1.6	30	150	-	-	<i>Short</i> [1979]
New Brunswick, Canada	straight	-	40	80	-	-	<i>Huntley</i> [1980]
Golfe du Lion, France	straight	≈0	80	130–550	10–110	-	<i>Barusseau and Saint-Guily</i> [1981]
HaHoterim, Israel	straight	0.3–0.6	70	30–500	-	-	<i>Goldsmith et al.</i> [1982]
Mediterranean, Israel	straight	0.3–0.6	100	175–300	-	-	<i>Bowman and Goldsmith</i> [1983]
Duck, NC, USA	straight	1.0–1.3	80	≈300	20–30	20	<i>Sallenger et al.</i> [1985]
Eastern Beach, Australia	straight	1.5	50	250	-	-	<i>Wright et al.</i> [1986]
Long Island, NY, USA	straight	0.6–1.5	60	≈2000	-	-	<i>Allen and Psuty</i> [1987]
Duck, NC, USA	straight	1.0–1.3	80	≈250	-	-	<i>Howd and Birkemeier</i> [1987]
Hald Strand, Denmark	straight	0.4	-	60–170	-	-	<i>Aagaard</i> [1988]
Lake Erie, Canada	straight (spit)	0	30	90–200	-	-	<i>Stewart and Davidson-Arnott</i> [1988]
Various, Denmark	mainly straight	≤0.4	40–170	30–1000	-	-	<i>Aagaard</i> [1989]
Cap-Ferret, France	straight	4.5	70	500–1000	-	-	<i>Froidefond et al.</i> [1990]
Terschelling, Netherlands	straight	1.2–2.8	220	1500–2000	-	-	<i>Ruessink</i> [1992]
Alexandria, Egypt	pocket	-	20–30	≈100	-	-	<i>Nafaa and Frihy</i> [1993]
Holland Coast, Netherlands	straight	1.2–1.9	120–150	1000–3000	-	-	<i>Wijnberg</i> [1995]
Egmond, Netherlands	straight	1.3–1.6	120	575	5–40	0–150	<i>Ruessink et al.</i> [2000]
Sand City, California, USA	straight	≈1	100	150	-	-	<i>MacMahan et al.</i> [2002]
Pomeranian Bay, Poland	straight	≈0	-	50–1000	-	-	<i>Furmanczyk et al.</i> [2002]
Truc Vert beach, France	straight	4.5	50	600	75	-	<i>Castelle et al.</i> [2003]
Noordwijk, Netherlands	straight	1.4–1.8	150	710–1360	0–30	0–180	<i>Van Enckevort and Ruessink</i> [2003]

<sup>a</sup>Specific examples include Gulf of Frejus, France and Castellabate, Gulf of Salerno, Italy.

however, no general ratio  $L/D$ , as reported literature values range between about 1 and 5–10. In addition,  $L$  has been suggested to depend on the water depth above the bar [*Clos-Arceduc*, 1962a], the bed slope [*Short*, 1979; *Barusseau and Saint-Guily*, 1981], and the cross-sectional area of the shoreward located bar trough [*Deigaard et al.*, 1999], with other more complicated parameters potentially playing a role [*Coco et al.*, 2002].

[4] Although the term “rhythmic” suggests that  $L$  varies little (if at all) alongshore, this appears to be the exception rather than the rule, in particular along straight beaches. For instance, *Rivière et al.* [1961] observed length variations between 100 and 250 m at Leucate Beach, France, and accordingly called crescentic bars “une quasi-périodicité”; *Aagaard* [1989] showed for various Danish sites that the ratio of the standard deviation in  $L$  to the alongshore-averaged  $L$  varied between 0.05 and 0.61; and *Furmanczyk et al.* [2002] found crescentic bars along the Pomeranian Bay (Baltic Sea, Poland) to have lengths between 50 and 1000 m. Information on the cross-shore amplitude  $A$  of crescentic bars, defined as half the cross-shore distance between consecutive horns and bays, is rather scarce; values up to 110 m have been reported (Table 1). Crescentic bars may migrate alongshore in the direction of wave advance [e.g., *Ruessink et al.*, 2000; *Van Enckevort and Ruessink*, 2003], suggesting the wave-driven alongshore current to be the dominant driving mechanism for alongshore bar migration. Maximum day-to-day migration rates  $c_m$  may be as high as 180 m/day (Table 1); longer-term migration rates are

likely to be substantially lower [*Homma and Sonu*, 1962; *Sonu*, 1968; *Greenwood and Davidson-Arnott*, 1975] because of the frequent reversals in the direction of wave advance and periods of no waves.

[5] Much of the existing field knowledge of crescentic bars relates to so-called bar state models developed for a microtidal single-bar setting [e.g., *Short*, 1979; *Wright and Short*, 1984; *Lippmann and Holman*, 1990]. In such models the full range of possible beach morphologies is classified into a limited number of discrete states. Crescentic bars are part of an accretional state sequence, developing from a straight shore-parallel bar within a few days following a period of storm or high swell waves. Under continuing low-energy conditions the horns weld to the shore, causing the disappearance of the alongshore continuous trough and the separation of the bays into isolated narrow cross-shore troughs with strong rip currents. This state, known as the transverse bar and rip state [*Wright and Short*, 1984] or as the (non)rhythmic attached bar state [*Lippmann and Holman*, 1990], generally forms within 1 to 2 weeks following peak wave events. If low-energy conditions continue to exist, the rips generally vanish while the bar welds to the shore completely, forming a low-tide terrace [*Wright and Short*, 1984]. With an increase in wave energy, an erosional state sequence sets in, often implying the almost immediate (within a day) destruction of the rhythmic features and a transition back to the shore-parallel bar-trough state. *Short and Aagaard* [1993] considered the single-bar state models also to be applicable to the inner bar in a multiple-bar system.

[6] Because bar state models utilize a coarse classification scheme, the temporal evolution of rhythmic bar length and amplitude is represented with abrupt steps. These steps are not accurate representation of the continuous evolution of the actual systems. Information on the dynamical nature of crescentic bars is needed to better understand the physical mechanism(s) leading to their generation and evolution [cf. *Phillips*, 1999]. Existing models on crescentic bars, reviewed briefly in section 2 of this paper, are based on fundamentally different concepts, yet they all predict wavelengths of the correct order of magnitude. In this sense the commonly stated success of any given concept to predict a form gives false confidence in the ability to understand the physical mechanism underlying crescentic bar behavior. However, when the dynamical nature of crescentic bars instead of their initial form is considered, differences in the model predictions emerge, opening up a more reliable way of concept testing.

[7] The aim of this paper is to analyze the temporal and spatial variability in crescentic bar behavior at four contrasting barred sites using high-resolution (hourly) long-term (months) video observations and to compare our results in a qualitative way to the temporal and spatial variability predicted by existing approaches and models for crescentic bar formation. We start off (section 2) with a brief description of these existing crescentic bar models, highlighting the differences in predicted behavior. The data we then analyze (sections 3 and 4) come from two single-barred beaches (Miyazaki, Kyushu, Japan, and Duck, North Carolina, USA) and two double-barred beaches (Gold Coast, Queensland, Australia, and Noordwijk, Netherlands). In section 5 we confront our findings to the spatial and temporal variability predicted by crescentic bar models, providing a qualitative test of the hypotheses underpinning these models. Finally, our main conclusions are summarized in section 6.

## 2. Crescentic Bar Models

[8] The intriguing (quasi-)rhythmicity of crescentic bars has led to a number of suggestions as to their origin. *King and Williams* [1949] considered crescentic bars within pocket beaches to form in response to two wave fields with approximately equal height arriving at more or less right angles to each other, each forming a transverse bar which would smooth together to a crescentic shape. Later on, *Clos-Arceuduc* [1962b] suggested that crescentic bars develop because of the interaction between standing wave systems, one oscillating between the headlands of a pocket beach and the other oscillating in the shore normal direction, and *Sonu* [1968] suggested that crescentic bars are bed perturbations related to the alongshore current, similar to dunes in rivers. Present-day crescentic bar models can be categorized as either template models or self-organization models [e.g., *Holman*, 2000; *Blondeaux*, 2001]. This distinction highlights a more fundamental difference on how to approach nearshore processes. In template models a three-dimensional pattern in the hydrodynamics (i.e., “the template”) forces the generation of a three-dimensional crescentic pattern in the morphology; there is no feedback between the hydrodynamics and the morphology. In contrast, in self-organization models crescentic features may be formed

through a positive feedback between the hydrodynamics (and sediment transport) and the morphology.

[9] In template models the template is the pattern of near-bed residual (or drift) velocities of low-mode monochromatic alongshore standing edge waves (waves bound to the coast by reflection and refraction) with a frequency in the infragravity (typically, 0.005–0.05 Hz) domain [*Bowen and Inman*, 1971; *Holman and Bowen*, 1982]. This pattern may arrange the sediment, stirred by short waves, into a crescentic bar with an alongshore wavelength equal to half the edge wavelength. The feedback between edge waves and the emerging crescentic bars is not considered. More recent theoretical work by *Chen and Guza* [1998] has shown that a low-mode edge wave progressive over a crescentic morphology may scatter a significant amount of incident low-mode edge wave energy in the same or opposite direction of the incident edge wave. The effect hereof on the preexisting morphology is, however, unknown. Essential requirements of the edge-wave template model are the presence of a significant amount of infragravity energy and the concentration of this energy in a single (dominant) frequency. Whereas this first requirement is generally satisfied in the field [e.g., *Guza and Thornton*, 1982; *Holman and Sallenger*, 1985; *Ruessink et al.*, 1998] (in particular during storms), the second requirement is generally not met [e.g., *Holman and Sallenger*, 1993; *Ruessink et al.*, 1998; *Holland and Holman*, 1999]; instead, infragravity (swash) spectra are generally white without any clear dominating frequency, which, as pointed out by *Holman and Sallenger* [1993], precludes bar formation. Edge wave trapping on alongshore currents or preexisting bars may circumvent the frequency selection problem [*Bryan and Bowen*, 1996], but the cross-shore convergence of drift of these trapped modes has been shown to be very small in comparison to other nearshore currents [*Bryan and Bowen*, 1997]. Accordingly, many do not consider template models to be responsible for crescentic bar formation anymore [e.g., *Bowen*, 1997; *Holman*, 2000]. Nonetheless, many textbooks on nearshore morphodynamics [e.g., *Komar*, 1998; *Woodroffe*, 2003] still indicate template models as the only feasible suggestion to the origin of crescentic bars.

[10] The formation of morphological patterns not directly mirroring the hydrodynamic forcing conditions is known as self-organization. This type of behavior has been mainly explored through linear stability analysis, numerical integration of the nonlinear momentum, and mass conservation equations and abstracted models. In linear stability models [e.g., *Hino*, 1974; *Christensen et al.*, 1994; *Deigaard et al.*, 1999; *Vittori et al.*, 1999; *Falqués et al.*, 2000; *Damgaard et al.*, 2002; *Klein et al.*, 2002; *Calvete et al.*, 2002; *Caballeria et al.*, 2003a], in all of which the flow is described by the depth-integrated equations for mass and momentum conservation, the time development of small periodic perturbations, superimposed on the forcing and/or the equilibrium morphology, is studied. This procedure is repeated for a range of perturbations differing in alongshore length evaluating, for each perturbation, the growth rate and the phase speed, which is a measure for the alongshore migration rate. The height of the perturbations is small to allow for a linearization of the model equations; accordingly, linear analysis is restricted to the initial development of crescentic bars. It is then assumed that the periodicity with the fastest

growth rate, which is typically  $O(10^2\text{m})$ , corresponds to the final configuration observed in nature. The growth of the perturbations is caused by a positive feedback mechanism between the hydrodynamics, sediment transport, and the evolving bathymetry which reinforces the initial perturbation. Apart from the model by *Vittori et al.* [1999], which is related to crescentic bars well outside the surf zone, the physical mechanism causing this feedback does not significantly differ among the various existing models and does not depend on the details of the hydrodynamic and sediment transport parameterization, which only affect growth rates and alongshore wavelength of the growing configuration(s). Generally, the smaller water depth at the positive perturbations locally reinforces wave breaking, generating an onshore flow over the perturbation to balance the cross-shore gradient in the radiation stress. Owing to the intensified wave breaking at the perturbation, the water level setup landward of the perturbation is larger than elsewhere. The resulting alongshore water level gradient generates an alongshore flow away from the perturbation, and where the alongshore flows meet, i.e., halfway between two perturbations, the water is pushed offshore. The perturbation thus causes a wave-driven circulation current with onshore flow over the positive perturbations and offshore flow over the negative perturbations. In combination with offshore increasing sediment transport rates [*Falqués et al.*, 2000], this circulation causes positive perturbations, associated with onshore flow, to grow into shoals or horns, while negative perturbations, associated with offshore flow, erode producing pools or bays. The alongshore alternation of pools and shoals is characteristic of a crescentic bar with an alongshore varying bar crest location. The effect of the perturbation on the wave-driven circulation is essentially the same for oblique wave incidence, but the circulation is superimposed on a mean wave-driven alongshore current, resulting in an meandering alongshore current [*Deigaard et al.*, 1999]. The meandering may be slightly out of phase with the bed perturbation owing to the inertia of the water particles, causing alongshore migration of the rhythmic morphology in addition to its growth [*Deigaard et al.*, 1999].

[11] Predictions of the amplitude development and analysis of the eventual interaction of individual crescents require nonlinear models. Modes other than the initially fastest growing may take over crescentic bar development, resulting in merging and splitting of individual perturbations. Thus, while linear models can only predict alongshore regular and temporally constant alongshore lengths, nonlinear models may produce spatial as well as temporal variability and, as such, result in morphological configurations that differ remarkably from those predicted by linear models. The spacing of the features is, again,  $O(10^2\text{m})$  and is found to scale with the surf zone width for a model characterized by an initially planar slope [*Caballeria et al.*, 2002]. In the case of an initially barred beach, the spacing of the crescentic features has been suggested to scale with the distance between the bar crest and the shoreline [*Damgaard et al.*, 2002], even though it seems likely that more complicated processes might operate and define the spacing in this case [*Coco et al.*, 2002]. The equations for the hydrodynamics and sediment transport do not substantially differ from those described for the linear

stability models apart from the model presented by *Reniers et al.* [2004], where wave-induced cross-shore sediment transport and wave group forcing have been included. Improvements in sediment transport parameterization resulted in similar alongshore spacings and faster growth rate of the features. The presence of infragravity waves results in smoother bathymetric changes but does not seem to be a prerequisite to generate alongshore patterns. The physical mechanism resulting in the development of crescentic bar morphology is essentially the same as discussed for linear models.

[12] In contrast to the models based on the depth-integrated equations for mass and momentum conservation discussed above, the abstracted model of *Coco et al.* [2000] focuses on the interactions and feedbacks of a shoreline/sandbar system using simplified sediment transport parameterizations resulting in a range of dynamics including the emergence of crescentic shapes. In the *Coco et al.* [2000] model, random alongshore variations are imposed in the cross-shore position and height of a triangular shaped bar on a sloping profile. The model predicts onshore (offshore) bar migration where the depth over the bar is smaller (larger) than average. During onshore (offshore) migration, the depths becomes even smaller (larger) and, accordingly the bar moves further onshore (offshore). Diffusion is included as a sort of alongshore flux over the bar crest to account for spatial coherence in its behavior. The bars will organize at a spacing that minimizes bar migration. In general, the model predicts the spacing of the crescentic features to scale with the distance between the bar and the shoreline. The combination of initially superimposed random variations and diffusion allows for separation and merging of the evolving crescentic bars. Thus, similar to the nonlinear models discussed above, interaction of individual crescentic features, which leads to temporal and spatial variability in crescentic bar behavior, is an essential outcome of the *Coco et al.* [2000] model.

### 3. Field Sites and Data Collection

[13] Crescentic-bar data analyzed in this paper were collected at the single-barred beaches near Duck, North Carolina, and Miyazaki, Kyushu, and at the double-barred beaches along the northern Gold Coast, Queensland, and Noordwijk (Table 2). Each of the sites is characterized by the presence of one or two alongshore sandbars that often develop crescentic planviews. Extensive site descriptions can be found in the work of *Lippmann and Holman* [1990] for Duck, *Suzuki et al.* [2002] for Miyazaki, *Turner et al.* [2000] for the Gold Coast, and *Van Enckevort and Ruessink* [2003] for Noordwijk. Environmental characteristics at the various sites are listed in Table 2 and include the mean slope  $\beta$  of the barred part of the profile, the median grain size  $D_{50}$ , the spring tidal range, and the offshore yearly averaged root-mean square wave height  $H_{\text{rms}}$  and peak period  $T_p$ . A cross-shore profile of each site is provided in Figure 1.

[14] At each site, data were collected hourly during daylight hours with a shore-based Argus video system [*Aarninkhof and Holman*, 1999] for the periods listed in Table 3. An Argus system typically comprises four or five video cameras that span a  $180^\circ$  view and allow full coverage of about 3–6 km (in the alongshore) of the

**Table 2.** Site Characteristics

Site	Setting	D50, $\mu\text{m}$	Slope, $1/\beta$	Tide, m	$H_{\text{rms}}$ , m	$T_p$ , s
Duck	single bar <sup>a</sup> near the the pier of the Corps of Engineers' Field Research Facility (FRF), facing Atlantic Ocean	180	80	1.1	0.63	9.1
Miyazaki	single bar <sup>b</sup> , north of Miyazaki harbor and breakwaters, facing Pacific Ocean	250	80	1.6	0.91	7.3
Gold Coast	double-barred beach, south of an artificial surfing reef [Turner <i>et al.</i> , 2000], facing Pacific Ocean	250	50	1.7	0.78	9.3
Noordwijk	double-barred beach on the Holland coast, facing North Sea	170	150	1.8	0.74	5.7

<sup>a</sup>Duck often shows the presence of two bars [e.g., Plant *et al.*, 1999], but the outer bar was not well developed during the period considered here (see Figure 1a) and was not visible on any of the analyzed plan view images.

<sup>b</sup>A broad breakerline during storms suggests the presence of an ephemeral outer bar.

nearshore. The cameras are mounted on a high viewpoint and are connected to a computer that controls image collection and communicates to the outside world by phone line. This, in combination with the automated nature of image collection and return, guarantees the collection of data with a high temporal resolution and long duration, making it an ideal data set to study the dynamical nature of crescentic bars. The image type used is the so-called time-exposure image, created by the averaging of 18000 individual snap-shot images ("photos") collected at the rate of 30 images/s for a period of 10 min.

[15] The images collected at the four sites were processed identically. For each hour the available images were rectified and merged to a single plan view image with a  $2.5 \times 2.5$  m grid. The rectification process is a transformation of all two-dimensional image pixel coordinates to three-dimensional (cross-shore, alongshore, vertical) world coordinates  $x$ ,  $y$ , and  $z$ . Because this transformation is under-determined,  $z$  was assumed to be constant and set equal to the (measured) offshore water level. The most conspicuous element of a plan view image is the presence of one or two alongshore continuous, white (high-intensity) bands that reflect the location of predominant wave breaking and offers a good proxy for the underlying sandbar morphology [Lippmann and Holman, 1989; Van Enckevort and Ruessink, 2001]. The alongshore varying pattern in a high-intensity band reflects the alongshore alternation of the bays (seaward perturbations) and shoals (shoreward perturbations) that are characteristic of crescentic bars [Ruessink *et al.*, 2000]. Images that lacked an alongshore high-intensity band because of the absence of breaking waves during low-energy conditions and images with poor visibility because of fog, rain, or sun glare were discarded from our data set. This limited the analysis to a total of 222, 262, 333/257, and 496/147 images at Duck, Miyazaki, Gold Coast (inner/outer bar), and Noordwijk (inner/outer bar), respectively (Table 3). From each selected plan view image the bar crest location was computed by sampling the cross-shore location of the breaking-induced intensity peaks alongshore, as detailed in the work of Van Enckevort and Ruessink [2001]. In this way a matrix  $X(t, y)$  was constructed for each site, consisting of bar crest positions  $X$  sampled at time  $t$  and alongshore location  $y$ . The alongshore extent of the bar crest lines at each site can be found in Table 3, as well as the largest gap between consecutive images, caused by rain (Gold Coast) or prolonged low-energy conditions (other sites).

[16] Before the temporal evolution of crescentic bars can be quantified from  $X(t, y)$ , four preprocessing steps are required, namely the removal of (1) the large-scale O(km)

shoreline trend, (2) the alongshore-averaged sandbar position, (3) the oblique orientation of the bar, and (4) the pixel-induced noise. The large-scale shoreline trend, which is constant for the periods considered here, was quantified for each site by the alongshore tracking of a shoreline break (i.e., the high-intensity maximum associated with wave breaking on the beach face) on one of the selected high-quality midtide images and the subsequent low-pass filtering of the sampled shoreline using the quadratic-loess interpolation method [Plant *et al.*, 2002] such that it contains only variance at length scales  $>3$  km. The data matrix from which the large-scale shoreline curvature is removed is henceforth referred to as  $D(t, y)$ . Time series of the alongshore-averaged sandbar position  $D_y(t)$  were simply computed as the alongshore average of each  $D(y)$  and were subsequently subtracted from  $D(t, y)$ . Then any oblique orientation of the bar was removed by subtracting the best linear line from each  $D(y) - D_y$ . The obliqueness was most pronounced for the outer bar at Noordwijk, related to a O(km) three-dimensional type of bar behavior [Wijnberg and Wolf, 1994] known as bar switching [Shand *et al.*, 2001]. Steps 2 and 3 result in the perturbation matrix  $\hat{D}(t, y)$ . An individual line from  $\hat{D}(t, y)$  will be referred to as a bar crest line in the following. Finally, pixel-induced noise was removed by low-pass filtering each bar crest line using the quadratic-loess interpolation method [Plant *et al.*, 2002]. At Duck and Miyazaki the minimum length scale preserved amounts to 150 m, at the Gold Coast (inner/outer

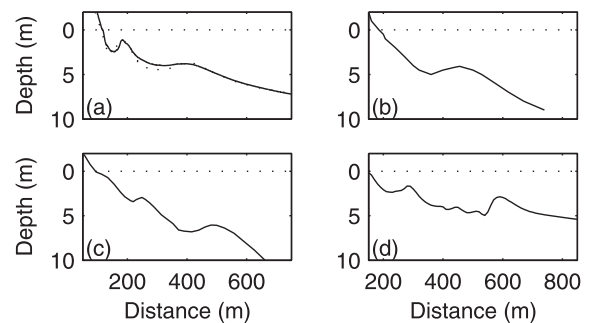


**Figure 1.** Depth versus cross-shore distance at (a) Duck (28 August 1998), (b) Miyazaki (1999), (c) the Gold Coast (6 September 1973), and (d) Noordwijk (29 July 2002). Note that the profiles in Figures 1b and 1d were surveyed well before the periods analyzed here and that the bars may thus be positioned at a different location than estimated from the Argus images. The solid (dotted) line in Figure 1a was measured north (south) of the FRF pier.

**Table 3.** Data Set Characteristics

Site	Period		$N_i^a$	$y_i^b$ m		Extent, km	$t_{\text{gap}}^c$ days
	DD-MM-YY	DD-MM-YY					
Duck	26-08-98	22-10-98	222	-1000	2350	3.35	8
Miyazaki	24-08-01	18-10-01	262	-500	2000	2.50	6
Gold Coast (inner)	14-01-03	18-04-03	333	-2100	500	2.60	3
Gold Coast (outer)	14-01-03	18-04-03	257	-2100	500	2.60	3
Noordwijk (inner)	25-01-02	12-11-02	496	-3000	2250	5.25	26
Noordwijk (outer)	25-01-02	09-11-02	147	-3000	3000	6.00	58

<sup>a</sup>Number of analyzed images.

<sup>b</sup>Alongshore coordinate in local Argus coordinate system.

<sup>c</sup>Largest gap between consecutive images.

bar) to 100/200 m, and at Noordwijk (inner/outer bar) to 300/600 m.

[17] From each smoothed bar crest line, every bay and horn were determined (Figure 2a) subject to the constraint that the cross-shore distance between a consecutive horn and bay was at least 5 m (for the outer bar at Noordwijk a 10-m constraint was used). This constraint was imposed to ensure that small, often short-lived wobbles were not detected as a crescentic bar; at the same time the constraint was sufficiently small to ensure that nonlinear behavior (e.g., merging and splitting of features), if present, was detected. For each crescentic bar, comprising two horns and an intermediate bay, the wavelength  $L$  was computed as the alongshore distance between the horns (Figure 2b), and the amplitude  $A$  was computed as half the average cross-shore distance between the bay and the two horns (Figure 2b). Finally, daily alongshore migration rates were computed by first averaging (in time) all bar crest lines of each day and by subsequently cross-correlating these daily averaged bar crest lines. The alongshore distance migrated by the crescentic bar pattern equals the magnitude of the lag at the positive peak closest to the origin of the cross-correlogram, whereas the sign of this lag indicates the migration direction. Estimates of migration rates influenced by bar splitting and/or merging were discarded because cross-correlation does not provide a good indication of migration rates.

#### 4. Results

[18] Space-time diagrams (timestacks) of the (low-pass filtered) perturbation matrices  $D(t, y)$  are shown for each site in Figures 3–6, together with time series of the alongshore-averaged sandbar position  $D_y$ , the alongshore-averaged wavelength  $L_y$  (i.e., the average of the lengths of all individual crescentic bars at each moment in time), and

the alongshore-averaged amplitude  $A_y$  (defined analogously to  $L_y$ ). Also shown in Figures 3–6 are time series of the measured offshore  $H_{\text{rms}}T_p$ , angle of incidence (relative to shore normal)  $\theta$ , and two parameters that have been suggested in the literature to determine beach state and the occurrence of crescentic bar systems  $\Omega = H_b/(T_p w_s)$  [Gourlay, 1968] and  $\Gamma = \epsilon\gamma(gH_b)^{0.5}/(4w_s)$  [Caballeria et al., 2002].  $H_b$  is the wave height at breaking, computed using linear wave theory assuming a cross-shore constant energy flux up to the point of breaking and a breaker angle of incidence of  $\approx 0$ ,

$$H_b = \left(\frac{\gamma}{g}\right)^{1/5} [H_{\text{rms}}^2 c_g \cos \theta]^{2/5}, \quad (1)$$

where  $c_g$  is the offshore group velocity and  $g$  is gravitational acceleration. The breaker parameter  $\gamma$  was set to 0.4 [Thornton and Guza, 1982]. The parameter  $\epsilon$  is a constant of  $O(0.01)$ , and  $w_s$  is the sediment fall velocity. In case  $\theta$  measurements were unavailable (Miyazaki),  $\theta = 0$  was assumed. Note that at the Gold Coast and Noordwijk,  $\Omega$  and  $\Gamma$  may not represent inner-bar values because wave breaking on the outer bar is not incorporated in equation (1). In the timestacks, light gray corresponds to negative perturbations (“horns”), while dark gray represents positive perturbations (“bays”). The vertical alternation of light and dark gray thus displays crescentic bars, whereas a general temporal shift in the bands (e.g., early March in the Gold Coast timestacks, Figure 5) reflects the alongshore migration of crescentic bars. The two white lines in the Duck timestack (Figure 3), located at  $\bar{D}(t, y) = 0$ , enclose the rather persistent bay related to the FRF pier; bar crest line information within this area, which varied in width from about 150 m to over 1000 m, was not used in any of

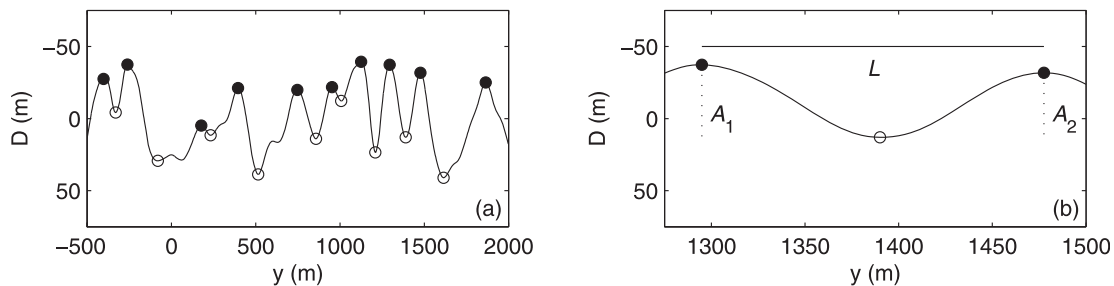


**Figure 2.** (a) Example of a bar crest line with detected (filled circles) horns and (open circles) bays. (b) A single crescent from Figure 2a with length  $L$  and amplitude  $A = 0.5 \times (A_1 + A_2)/2$ .

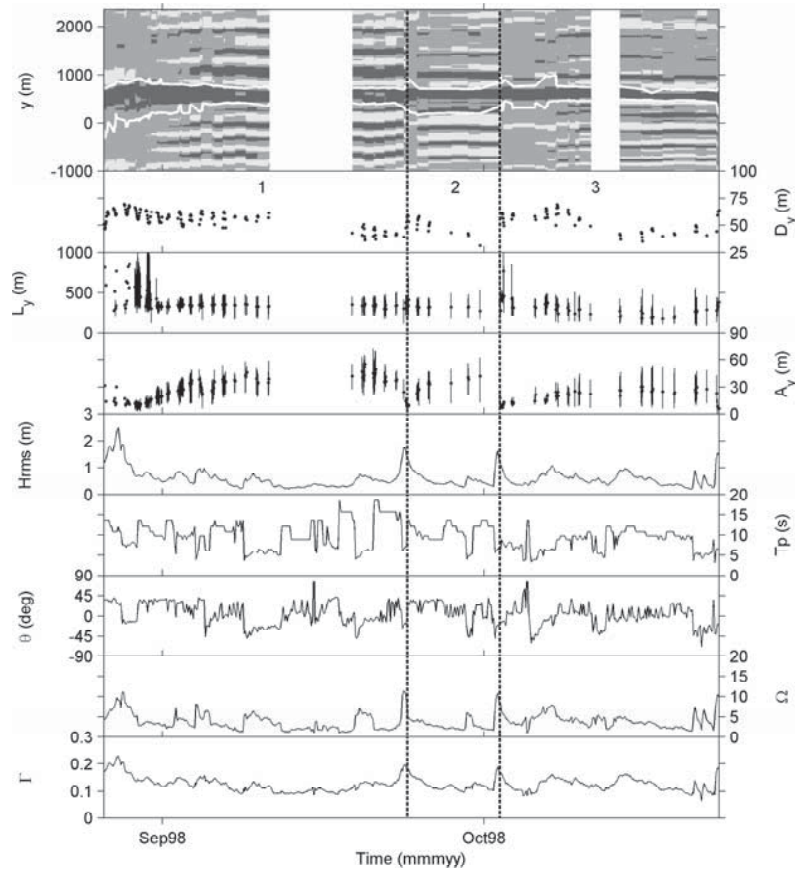


**Figure 3.** Time series of (from top to bottom) the bar crest lines  $\tilde{D}(y)$ , alongshore-averaged sandbar position  $D_y$ , alongshore-averaged wavelength  $L_y$  (dots), alongshore-averaged amplitude  $A_y$ , offshore root-mean square wave height  $H_{rms}$ , peak period  $T_p$ , angle of incidence  $\theta$  relative to shore normal, nondimensional fall velocity  $\Omega$ , and the parameter  $\Gamma$  at Duck. In the upper plot, referred to in the text as a space-time diagram or timestack, dark shading corresponds to positive perturbations (“bays,”  $\tilde{D}(t, y) \geq 10$  m), light shading represents negative perturbations (“horns,”  $\tilde{D}(t, y) \leq -10$  m), and medium shading relates to  $-10 < \tilde{D}(t, y) < 10$  m. White vertical bands correspond to missing data extending for more than 2 days. The vertical lines in the  $L_y$  and the  $A_y$  panels run from the minimum to the maximum value of  $L$  and  $A$  observed in each bar crest line. The vertical dashed lines correspond to moments when an existing crescentic pattern is wiped out and a new pattern appears.

the Duck results presented below. Tidal  $D_y$  variations of about 5–15 m reflect tidal water level induced variations in the location of the breaker zone with respect to the underlying sandbar morphology rather than true on/offshore bar migration [Van Enckevort and Ruessink, 2001].

[19] As can be seen in Figures 3–6 and Table 4, considerable intrasite and intersite variability exists for  $L_y$ . For instance,  $L_y$  at Duck ranged from about 170 to 850 m (Table 4), roughly the minimum  $L_y$  observed for the outer bar at Noordwijk, where the maximum detected  $L_y$  exceeded 2 km (Table 4). At most sites,  $A_y$  ranged from about 10–20 to 50–70 m, except at the inner bar at the Gold Coast, where the maximum  $A_y$  amounted to about 30 m only (Table 4). Alongshore migration rates  $c_m$  were typically less than 40 m/day (Table 4). Ratios  $L_y/D_y$  had data set-averaged values between 3.0 (Gold Coast, inner bar) and 9.6 (Noordwijk, inner bar); minimum and maximum  $L_y/D_y$  were 1.6 and 25.3, respectively (Table 4).

[20] In general terms the temporal development of the crescentic bars at the two single-barred beaches (Duck and

Miyazaki) and at the outer Gold Coast bar was quite similar. During each high-energy event (typically,  $H_{rms} > 1.5$ – $2.5$  m,  $\Omega > 7$ – $10$ ,  $\Gamma > 0.13$ – $0.20$ ), preexisting crescentic bars were wiped out (Figure 7a, referred to in the following as a morphological reset), and in an alongshore averaged sense the bar moved offshore by some 20–40 m. Within 1–3 days after the peak of the storm, low-amplitude ( $A_y < 20$  m) large-wavelength ( $L_y \sim 500$ – $750$  m) crescents appeared (Figure 7b), with  $L_y/D_y \sim 7$ – $10$ . Within the next few days, new crescents formed in between some of the existing large crescents (Figure 7c), causing  $L_y$  and  $L_y/D_y$  to decrease to typical values of  $\approx 300$ – $400$  m and  $\approx 2$ – $6$  (depending on the site, see mean  $L_y/D_y$  in Table 4), respectively. Whereas  $L_y$  usually remained approximately the same during the remainder of the lifetime of the crescentic bars,  $A_y$  increased to a maximum value of 40–60 m, after which  $A_y$  could reduce slightly (see, e.g., April 2003 at the Gold Coast). Usually, the crescentic bars reached their maximum amplitude some 1.5–3 weeks after the peak of the storm (maximum  $A_y$  growth rates are 5–

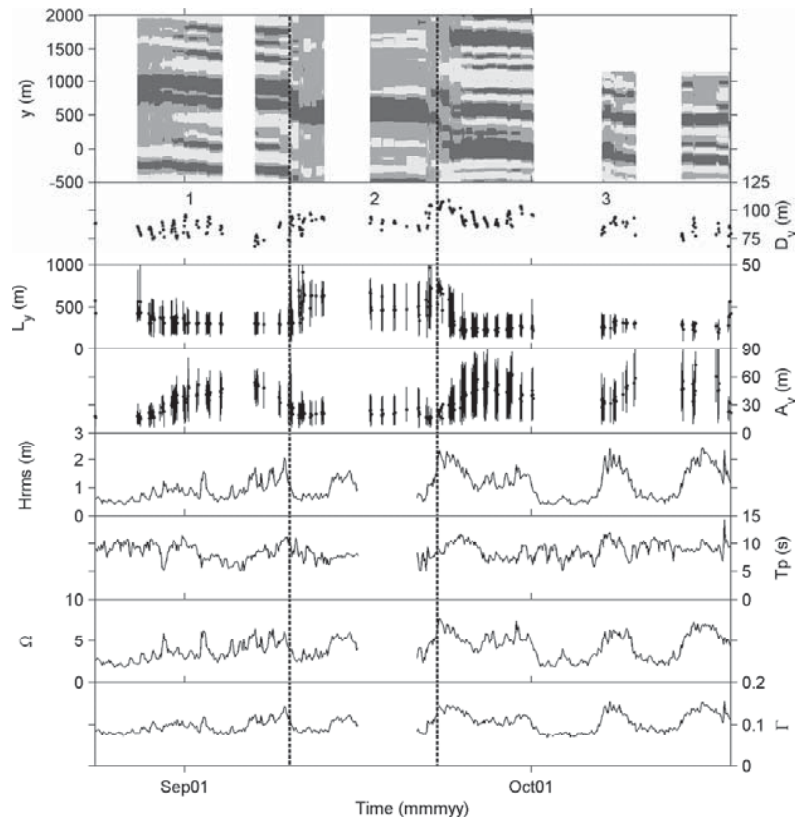


**Figure 4.** Time series of (from top to bottom) the bar crest lines  $\tilde{D}(y)$ , alongshore-averaged sandbar position  $D_y$ , alongshore-averaged wavelength  $L_y$  (dots), alongshore-averaged amplitude  $A_y$  (dots), offshore root-mean square wave height  $H_{rms}$ , peak period  $T_p$ , nondimensional fall velocity  $\Omega$ , and the parameter  $\Gamma$  at Miyazaki. In the upper plot, dark shading corresponds to positive perturbations (“bays,”  $\tilde{D}(t, y) \geq 10$  m), light shading represents negative perturbations (“horns,”  $\tilde{D}(t, y) \leq -10$  m), and medium shading relates to  $-10 < \tilde{D}(t, y) < 10$  m. White vertical bands correspond to missing data extending for more than 2 days. The vertical lines in the  $L_y$  and the  $A_y$  panels run from the minimum to the maximum value of  $L$  and  $A$  observed in each bar crest line. The vertical dashed lines correspond to moments when an existing crescentic pattern is wiped out and a new pattern appears.

7 m/day), which at Duck and Miyazaki coincided with the welding ashore of several horns and the transition of the “crescentic bar state” into the “transverse bar and rip state” (Figure 7d). The welding ashore of some horns in the outer Gold Coast bar was observed only once (mid-April 2003), some 6 weeks after their initial formation. During the entire period following the storm, the bars at the three sites moved onshore slowly with typical rates of 0.5–1 m/day, causing a slow increase in  $L_y/D_y$ . The next storm destroyed the crescentic shapes and forced the bars to move offshore again (Figure 7e). At all three sites we observed three such periods comprising crescentic bar birth, growth, and decay (Figures 3–5).

[21] At first glance the observations for the inner bar at the Gold Coast and for both Noordwijk bars differ considerably from those described in the previous paragraph. However, these differences might be an expression of a different relaxation time (the timespan between the onset of morphological change and attainment of equilibrium [De Boer, 1992]) relative to the characteristic timescale of the forcing (say, the timespan between consecutive storms). For the inner Gold Coast bar the relaxation time is rather short:

the “crescentic bar state” lasted only for 1–2 days and the accretional bar state development (section 1) continued all the way to the rather featureless “low tide terrace” state. During each high-energy event, the inner bar became separated from the beach by a trough, visible as an alongshore continuous region of low intensity (Figures 8a and 8e). Within, say, 2 days, alongshore nonuniformities emerged (Figure 8b), which, at that moment, usually had larger amplitudes than the features in the outer bar. In comparison to the crescentic shapes that developed later on in the outer bar, the inner-bar shapes had rather narrow bays and wide horns (cf. Figure 8b to Figure 8d). Within another day or so the inner bar merged to the shore and developed into a rip-cut low-tide terrace (Figure 8c). At this time,  $A_y$  was  $\approx 20$ –30 m and did not increase any further. As time progressed and low-energy conditions continued to exist, some rips vanished whereas others appeared (e.g., Figure 5, periods 2 and 3); occasionally, most rips vanished altogether, leaving the low-tide terrace almost featureless (Figure 8d), whereas at the same time the crescentic bars in the outer bar were well developed. In such a situation, inner-bar  $L_y$  was larger than outer-bar  $L_y$ ; see, e.g., mid-March

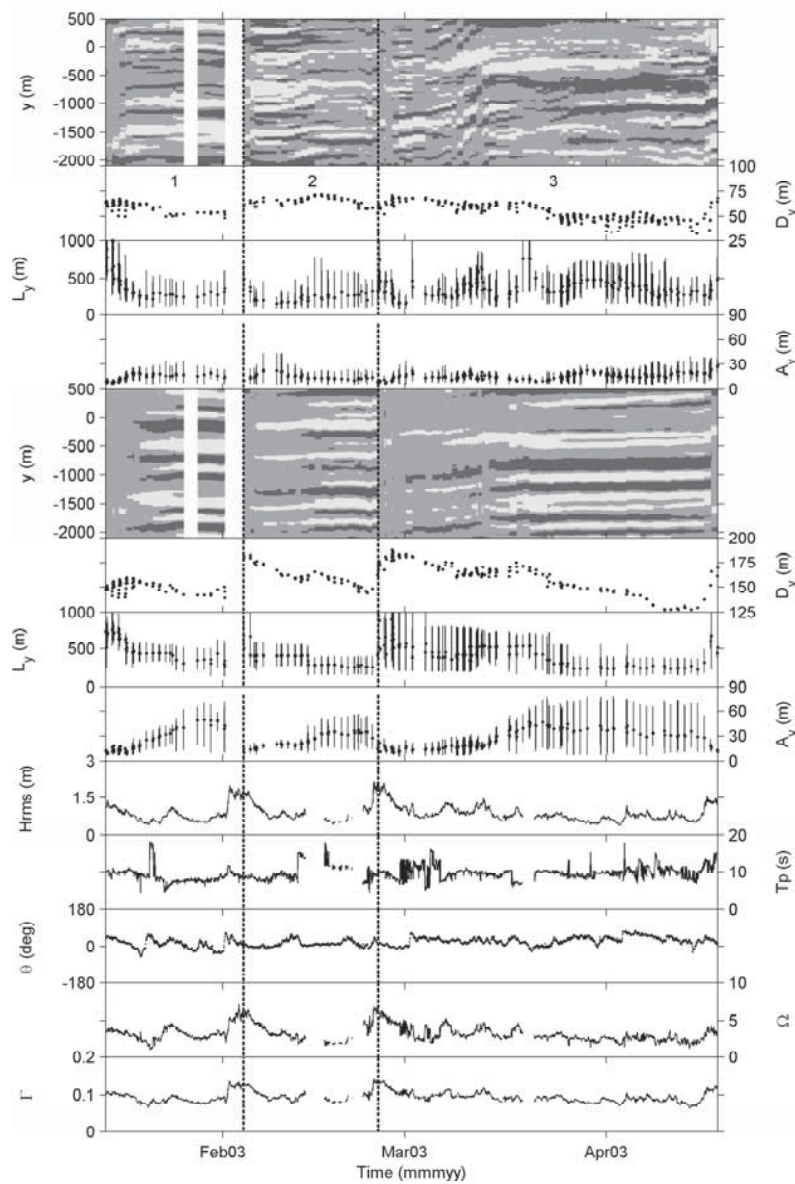


**Figure 5.** Panels 1–4 are inner-bar time series of (from top to bottom) bar crest lines  $\tilde{D}(y)$ , alongshore-averaged sandbar position  $D_y$ , alongshore-averaged wavelength  $L_y$  (dots), and alongshore-averaged amplitude  $A_y$  (dots) at the Gold Coast. Panels 5–8 show the same information as panels 1–4 but now for the outer bar. The remaining panels are time series of (from top to bottom) offshore root-mean square wave height  $H_{rms}$ , peak period  $T_p$ , angle of incidence  $\theta$  relative to shore normal, nondimensional fall velocity  $\Omega$ , and the parameter  $\Gamma$ . In the inner-bar timestack (panel 1), dark shading corresponds to positive perturbations (“bays,”  $\tilde{D}(t, y) \geq 5$  m), light shading represents negative perturbations (“horns,”  $\tilde{D}(t, y) \leq -5$  m), and medium shading relates to  $-5 < \tilde{D}(t, y) < 5$  m. In the outer-bar timestack (panel 5) the boundaries between light and medium shading and between medium and dark shading are  $-10$  m and  $10$  m, respectively. White vertical bands correspond to missing data extending for more than 2 days. The vertical lines in the  $L_y$  and the  $A_y$  panels run from the minimum to the maximum value of  $L$  and  $A$  observed in each bar crest line. The vertical dashed lines correspond to moments when an existing crescentic pattern is wiped out and a new pattern appears.

until early April 2003 in Figure 5. The inner-bar timestack in Figure 5 suggests that the few remaining rips in the low-tide terrace were remnants of preexisting rips; see also *Wright and Short* [1984]. During the next storm the low-tide terrace was destroyed, causing the reappearance of the inner bar trough (Figure 8e). A more extensive comparison

of inner- and outer-bar behavior at the Gold Coast will be the focus of another paper.

[22] In contrast, the relaxation time at Noordwijk is long relative to the relaxation times at the other sites. In fact, it is of sufficiently long duration that the crescentic features in both Noordwijk bars appeared insensitive to the offshore

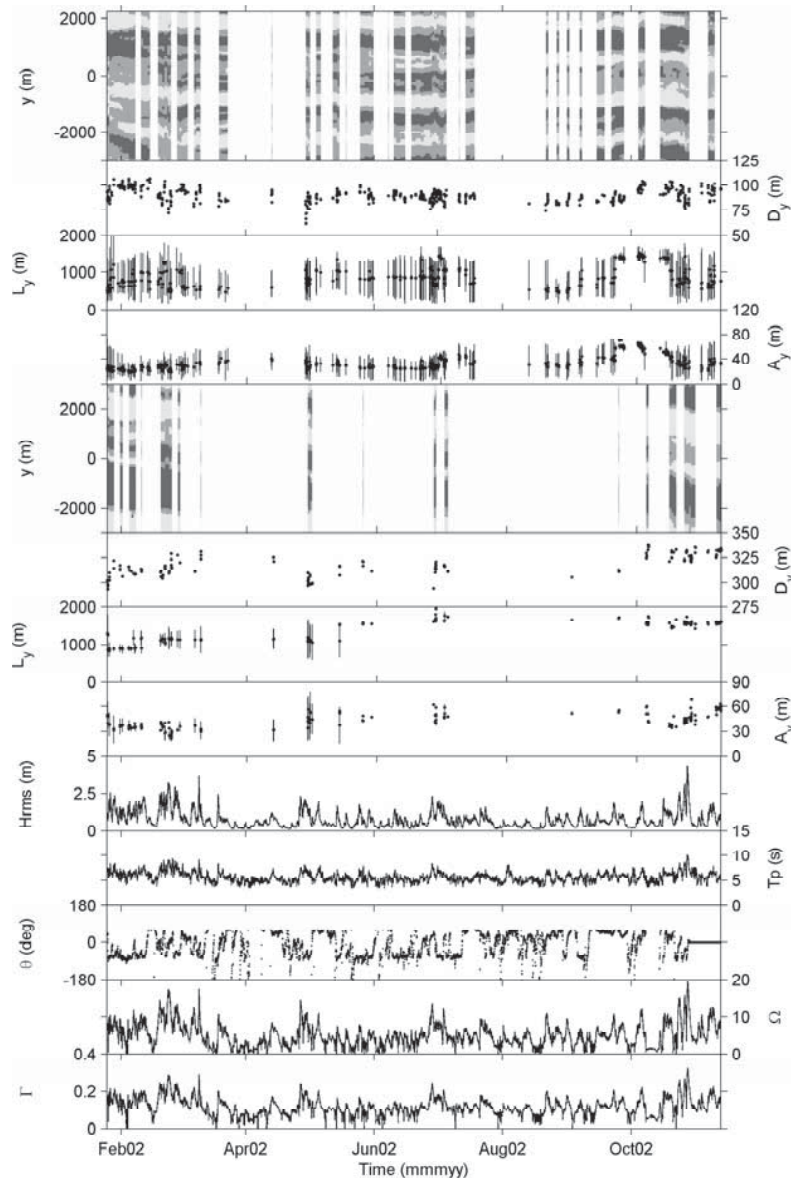


**Figure 6.** Panels 1–4 are inner-bar time series of (from top to bottom) bar crest lines  $\tilde{D}(y)$ , alongshore-averaged sandbar position  $D_y$ , alongshore-averaged wavelength  $L_y$  (dots), and alongshore-averaged amplitude  $A_y$  (dots) at the Noordwijk. Panels 5–8 show the same information as panels 1–4 but now for the outer bar. The remaining panels are time series of (from top to bottom) offshore root-mean square wave height  $H_{rms}$ , peak period  $T_p$ , angle of incidence  $\theta$  relative to shore normal, nondimensional fall velocity  $\Omega$ , and the parameter  $\Gamma$ . In both timestacks (panels 1 and 5) dark shading corresponds to positive perturbations (“bays,”  $\tilde{D}(t, y) \geq 10$  m), light shading represents negative perturbations (“horns,”  $\tilde{D}(t, y) \leq -10$  m), and medium shading relates to  $-10 < \tilde{D}(t, y) < 10$  m. White vertical bands correspond to missing data extending for more than 2 days. The vertical lines in the  $L_y$  and the  $A_y$  panels run from the minimum to the maximum value of  $L$  and  $A$  observed in each bar crest line.

**Table 4.** Statistics of  $L_y$ ,  $A_y$ ,  $c_m$ , and  $L_y/D_y$ .

Site	$L_y$ , m			$A_y$ , m			$c_m$ , m/day		$L_y/D_y$		
	Minimum	Mean	Maximum	Minimum	Mean	Maximum	Minimum	Maximum	Minimum	Mean	Maximum
Duck	173	365	855	6	24	55	−40	60	3.9	6.7	17.6
Miyazaki	200	363	966	13	34	72	−50	30	2.2	4.1	10.2
Gold Coast (inner)	151	373	1528	7	15	28	−35	45	2.2	6.8	25.3
Gold Coast (outer)	224	483	1608	8	24	49	−30	35	1.6	3.0	11.2
Noordwijk (inner)	441	871	1503	17	36	71	−55	60	4.8	9.6	17.3
Noordwijk (outer)	828	1369	2120	22	43	68	−20	25	2.7	4.3	6.7

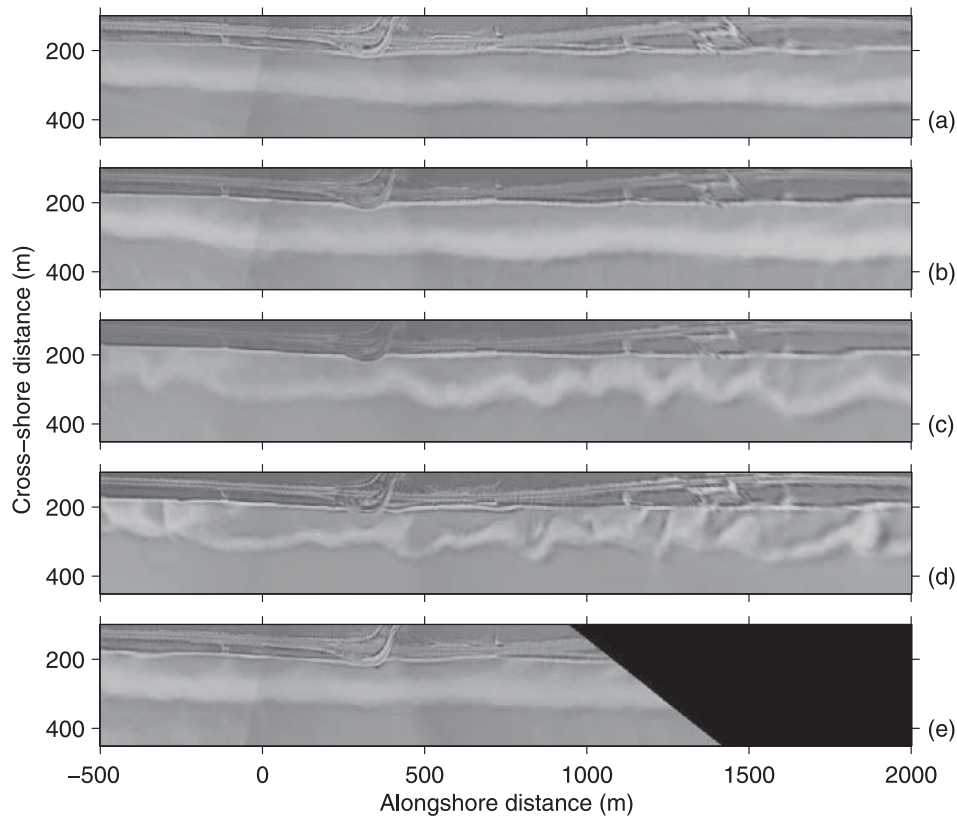


**Figure 7.** Plan view images on (a) 22 September 2001 0700 UT, (b) 23 September 2001 0700 UT, (c) 25 September 2001 0100 UT, (d) 1 October 2001 0200 UT, and (e) 19 October 2001 0600 UT at Miyazaki, showing the temporal development of crescentic bars; see text for further explanation.

forcing, not showing clear patterns of generation, growth, and decay in response to changes in the offshore wave height as observed at the other sites. At the inner Noordwijk bar, for instance, crescentic bars with a length of some 1500 m can be followed for the entire 10-month duration of the period considered (Figures 6 and 9). Even the strongest storm in a decade (late October 2002) with  $H_{rms} \sim 4.5$  m,  $\Omega \sim 20$ , and  $\Gamma \sim 0.3$  did not result in a total morphological reset. Also, the inner bar did not migrate offshore and onshore in response to storms and prolonged low-energy conditions as at the other sites; instead, inner-bar  $D_y$  showed a weak seasonal trend, with some 10–20 m more shoreward positions in the summer months. Occasionally, smaller-scale ( $L \sim 500$  m) features developed mainly in the bays of the  $\approx 1500$  m features (Figure 9). These secondary features generally developed following a succession of high-energy events (e.g., late March 2002; see Figures 6 and 9b) and gently disappeared during the next succession of storms (e.g., mid-May 2002, see Figures 6 and 9c); individual storms, each of which with  $H_{rms}$ ,  $\Omega$ , and  $\Gamma$  high enough to straighten the bars at the other sites completely, however, did not notably effect these secondary features. Potential reasons for the different relaxation times at the various sites are discussed in section 5.

[23] At none of the sites the crescentic bar patterns were truly rhythmic as in virtually every crest line the ratios between the maximum and minimum wavelength and between the maximum and minimum amplitude exceeded

a factor of 2. Similarly, the growth in time of individual crescents showed complicated behavior with  $L$  changing over time. An example hereof for Duck (period 1) is shown in Figure 10. Notice how the length of the first crescent  $L$  gently decreased in time, of the second remained about constant, and of the third (at least initially) more than doubled. A second example (Gold Coast, outer bar) is provided in Figure 11. Whereas the wavelength of the first crescent remained about constant, the length of the second one suddenly halved near 14 February 2003, caused by the splitting of this crescent into half.

[24] Figures 7, 9, 10, and 11 emphasize that crescentic bars may undergo considerable temporal changes, including splitting and merging of individual crescents, that result in morphological configurations that differ remarkably from those formed initially after a storm. The splitting and merging of crescents was observed at each site but was most ubiquitous at the Gold Coast (e.g., Figure 12), where a total of 13 (20) splitting and 4 (12) merging events were observed in the outer (inner) bar. Therefore the Gold Coast data were analyzed in more detail to determine whether there was any systematics to the when and where of this form of nonlinear behavior. As can be seen in Figure 13, splitting and merging events were observed for almost all wave heights less than the ones that would result in a full reset of the system. In more detail, most merging events took place during an increase in wave height, whereas most splitting events were observed during a decrease in wave

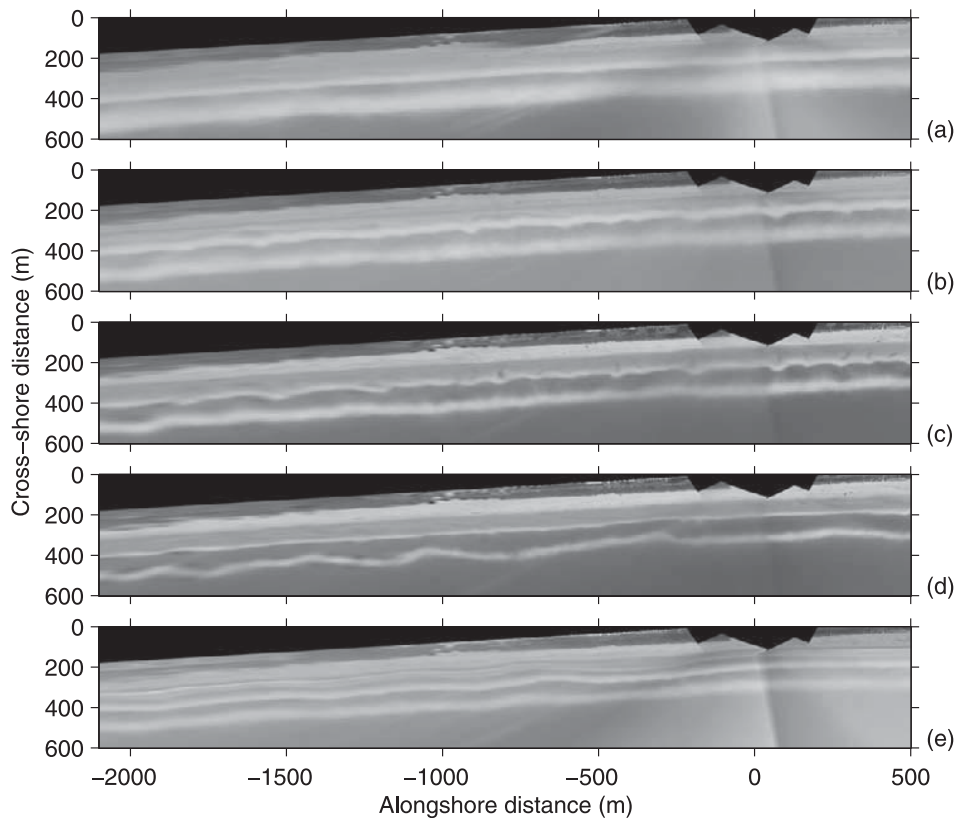


**Figure 8.** Plan view images on (a) 25 February 2003 2300 UT, (b) 27 February 2003 0600 UT, (c) 1 March 2003 0400 UT, (d) 19 March 2003 0300 UT, and (e) 21 April 2003 2200 UT at the Gold Coast, showing the temporal development of alongshore nonuniformities in the inner bar; see text for further explanation.

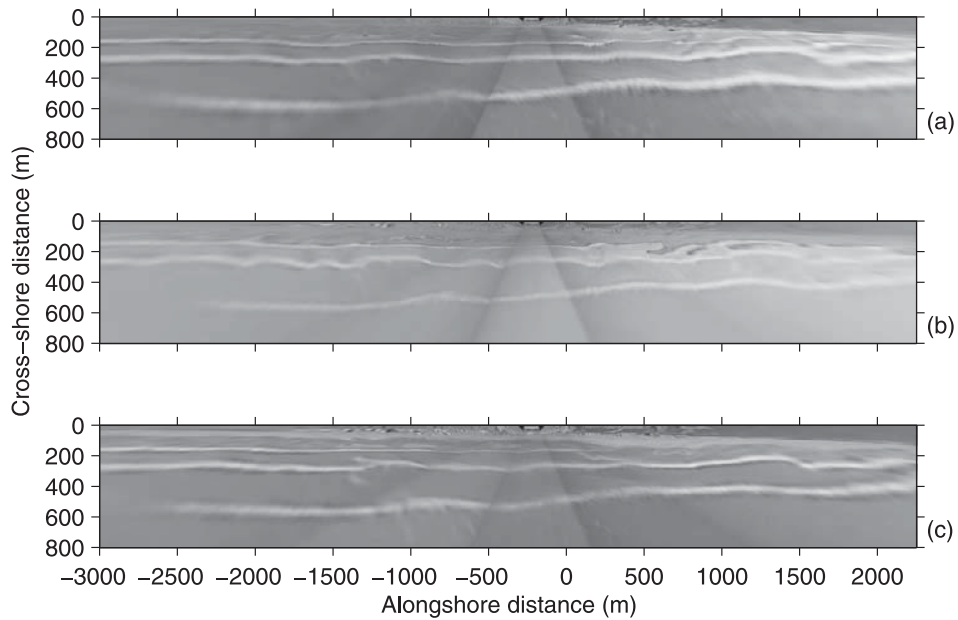


**Figure 9.** Plan view images on (a) 28 February 2002 1200 UT, (b) 20 March 2002 1300 UT, and (c) 14 May 2002 1000 UT at Noordwijk, showing the temporal development of crescentic shapes in the inner bar ( $x \approx 250$  m); see text for further explanation. In Figure 9b, secondary features are particularly obvious around  $y = -2750$ ,  $-1500$ , and  $-750$  m. Notice the similarity in inner-bar crescents in Figures 9a and 9c.

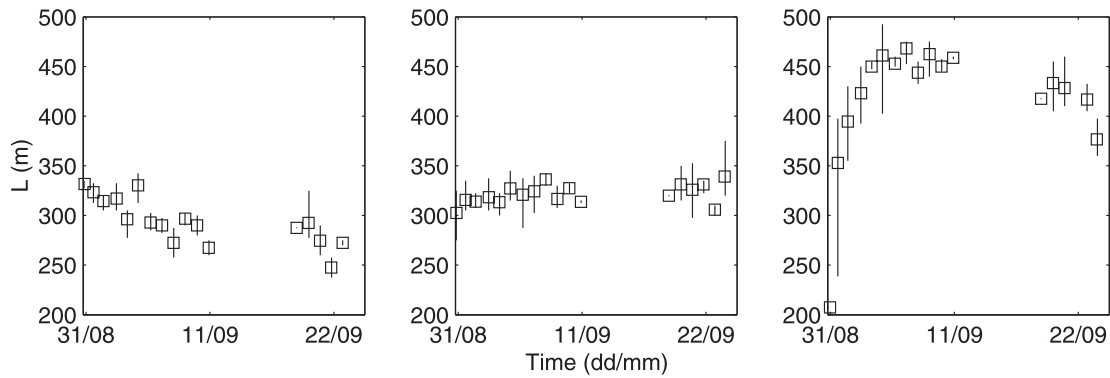


**Figure 10.** Wavelength  $L$  of three crescentic bars at Duck for the same time period. The symbols represent daily average values, and the vertical lines are daily maximum and minimum values.

height. This is qualitatively consistent with the observations in Figures 7b–7c and 9. Also, there is the tendency that it is the largest crescentic bar to split (for the inner bar, 80% of the splits take place in the largest crescent bar; this number amounts to 69% for the outer bar). Similarly, crescentic bars with smaller lengths (relative to  $L_y$ ) usually merge into a larger crescentic bar system (for the inner (outer) bar this is the case for 92 (100)% of the observations). Both splitting and merging thus appear to indicate that the crescentic bar system tends to self-organize into a more uniform spacing.

## 5. Discussion

[25] In this section the video observations presented in the preceding figures and discussion are used to test some of the hypotheses underpinning existing approaches and models for crescentic bar formation (section 2). The template approach is difficult to test because, at present, there is no model to describe the temporal evolution of morphology under edge wave forcing and how morphology might feed back on edge waves. Nevertheless, crescentic bars are observed (e.g., Figure 7) to develop mainly during calm conditions (when infragravity energy is usually relatively low) and to be smoothed out during storm conditions (when infragravity energy is usually a significant fraction of the total wave energy [Guza and Thornton, 1982]). Further-

more, the template approach does not in principle allow for the commonly observed merging and splitting events between crescentic systems (Figures 12 and 13). Of course, as already suggested for beach cusps [Inman and Guza, 1982], the assumption that edge waves only provide the initial perturbation of the seabed could be made but such an assumption would significantly reduce the role of edge waves to just one of the many possible sources of morphodynamic instability. Finally, observations indicate significant changes in the alongshore spacing of crescentic bars, while the template model assumes the appearance of a more regular, periodic, morphological pattern.

[26] In many cases the validity of linear stability models is implied through comparisons between the wavelength of the fastest growing mode and some average final spacing observed in the field. This study indicates that observed initial  $L_y$  (e.g., Figure 4b) and  $L_y/D_y$  may be a factor of 2 larger than the observed final  $L_y$  (e.g., Figure 4c) and  $L_y/D_y$ . Also, wavelength variations over time and space are very common (Figures 7–13), and observed final spacings are the result of intrinsically nonlinear interactions (merging and splitting). Furthermore, there is not a consistent method for comparing predictions to observations because, in contrast to model assumptions, natural conditions are changing rapidly and the initial morphological configuration is already significantly perturbed. Although, as observed in

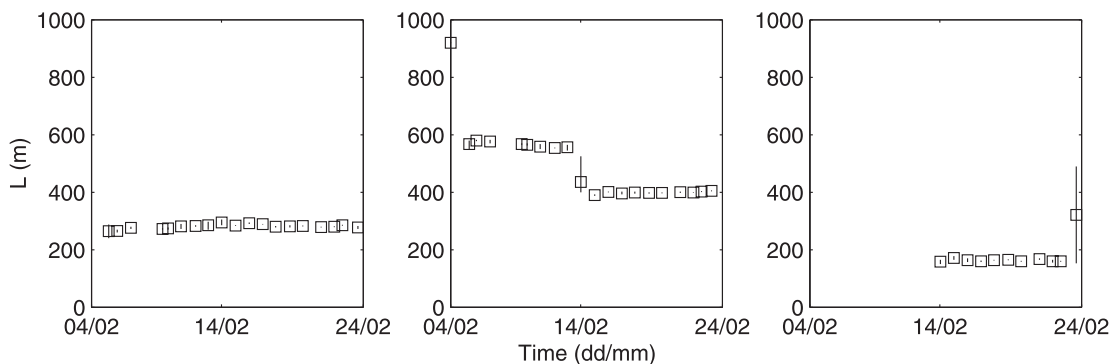


**Figure 11.** Wavelength  $L$  of three crescentic bars at the Gold Coast (outer bar) for the same time period. The symbols represent daily average values, and the vertical lines are daily maximum and minimum values. The sudden decrease in  $L$  of the second crescent is caused by its splitting into half. The length of the new crescent is shown in the third panel.

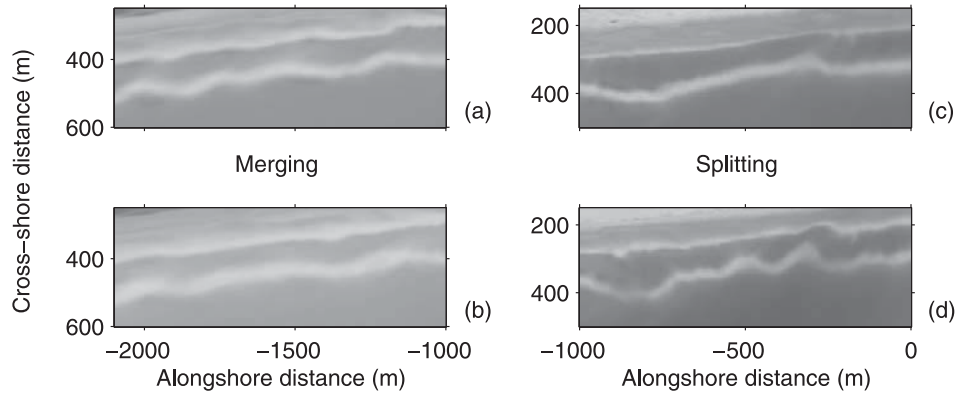


**Figure 12.** Example of the (left) merging and (right) splitting of individual crescents in the outer bar at the Gold Coast. In the merging event the crescent with its bay near  $y = -1650$  m vanished, whereas in the splitting event a new crescent developed between  $y = -500$  and  $-650$  m. Images were collected on (a) 11 March 2003 0700 UT, (b) 12 March 2003 0700 UT, (c) 19 March 2003 0500 UT, and (d) 26 March 2003 0000 UT.

numerical experiments [Calvete and de Swart, 2003], the possibility that the finite amplitude spacing of morphological features is the same as the one of the fastest growing mode cannot be dismissed entirely; the predictive role of models based on linear stability analysis should probably be reduced to the identification of the physical processes and conditions that might lead to crescentic bar development. Analyzing in more detail some of the linear stability analysis models, the model presented by Vittori *et al.* [1999], assuming the development of crescentic features offshore of the breaking zone, does not relate to the present study where the features are observed to develop exactly in the breaking zone.

[27] Although nonlinear models are potentially better suited for comparisons to field observations, they still rely on assumptions such that only qualitative comparisons are allowed. Unlike the present field observations, initial models described the emergence of crescentic features on an initially planar profile [Caballeria *et al.*, 2002]. Such a model could only be used to test if the mechanisms unravelled by linear stability analysis also operated in the nonlinear field. Later advances [Damgaard *et al.*, 2002; Coco *et al.*, 2002] have overcome this problem but still struggle to reach nontrivial equilibrium configurations, and no merging or splitting of crescentic systems could be detected that was unequivocally unrelated to the presence of a finite domain (in the alongshore direction) [Caballeria *et al.*, 2003b]. Further developments are needed like inclusion of more realistic hydrodynamic conditions (most models still use monochromatic forcing) to compare growth rates and spacing variability and a sediment transport parameterization that allows to simulate full sandbar dynamics (e.g., onshore/offshore migration) rather than just crescentic bar development. Predictions from such nonlinear models, of which Reniers *et al.* [2004] is an example for embayed beaches, can be treated in a similar manner as field observations, with the same wave conditions and the same initial bathymetry.

[28] The different timescales of crescentic bar evolution, as observed in section 4, suggest that the relaxation times (approximately the reciprocal of growth rate) at the four sites are different. Relaxation time, defined by De Boer [1992,

p. 307], as “the timespan between the onset of morphological change and attainment of equilibrium corresponding to the new process conditions,” increases with increasing spatial scale, as it depends on the amount of material that has to be

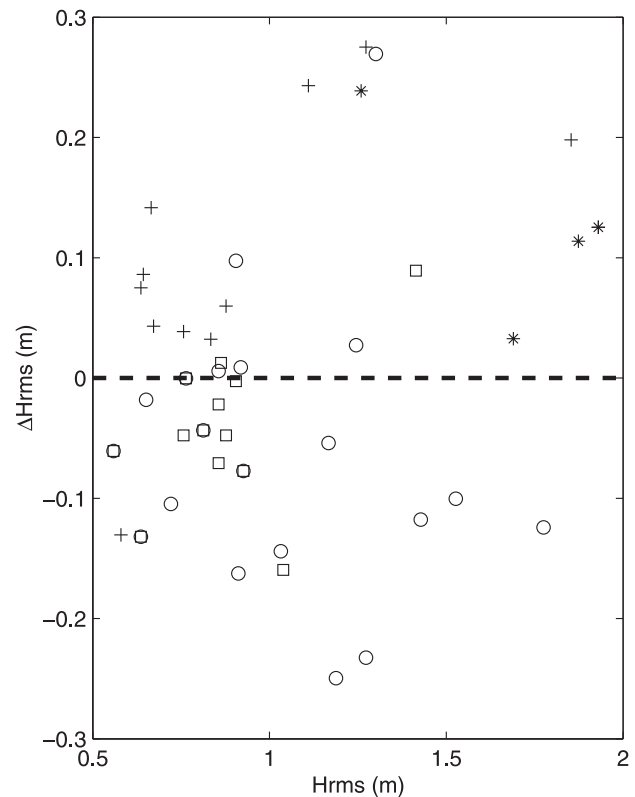


**Figure 13.** Merging (asterisk, outer bar; pluses, inner bar) and splitting (squares, outer bar; circles, inner bar) events at the northern Gold Coast as a function of the offshore root-mean square wave height  $H_{rms}$  and the change in  $H_{rms}$ ,  $\Delta H_{rms}$ . The  $H_{rms}$  values on the x-axis are the  $H_{rms}$  values when a crescentic bar was observed for the last (first) time in case of merging (splitting). The  $\Delta H_{rms}$  is the difference between the actual  $H_{rms}$  and the value 24 hours before.

transported to attain equilibrium and on the sediment transport rates [Cowell and Thom, 1994]. Linear stability analyses carried out by Caballeria *et al.* [2003a, 2003b] showed the growth rate to increase (or the relaxation time to shorten) with an increase in the water depth in the trough and a decrease in the depth over the bar. Also, an increase in wave height was found to increase the growth rate. In all cases the authors ascribed the increasing growth rate to a more intense circulation pattern (either by a decrease in friction in the trough or an increase in wave breaking across the bar), which can be interpreted as larger sediment transport rates.

[29] As mentioned above, sediment transport rates are only part of the story in explaining differences in temporal evolution of crescentic sandbars as the volume of sand contained in the bar also plays a role. Even if the sediment transport rates at the inner Gold Coast bar and the inner Noordwijk bar are the same, it would still take far more time for crescentic bars to develop and evolve at Noordwijk than at the Gold Coast (compare depth profiles in Figures 1c and 1d). We hope that these observations provide sufficient rules of thumb to test self-organization models in an exploratory way [cf. Murray, 2003], thereby proving or refuting the hypotheses underpinning these models.

## 6. Conclusions

[30] Hourly time exposure images collected at four barred beaches (Duck, Miyazaki, Gold Coast, and Noordwijk) have shown that crescentic sandbar wavelength and amplitude variations over space and time are very common. At any moment in time the wavelength of the smallest and longest crescentic bar can differ by a factor of 2; this also holds for crescentic bar amplitude. Temporal changes in wavelength and amplitude result from merging and splitting of individual crescents, causing the “final” configuration of a crescentic sandbar system to be different from the initial configuration. For instance, our observations indicate that initial wavelength may be a factor of 2 larger than the final wavelength. As indicated by the Gold Coast data, merging and splitting are an attempt of the crescentic bar system to self-organize into a more uniform pattern, as splitting is usually confined to the longest crescentic bar observed, whereas merging usually combines the smallest crescentic bars into a longer bar. The timescale of crescentic bar development differs considerably between the sites: whereas crescentic patterns in the inner Gold Coast bar exist for a few days only (and then merge to the beach), patterns in the Noordwijk bars have lifetimes exceeding the length of the data set (10 months) and even survived the strongest storm in a decade with offshore root-mean square wave heights of some 4 m. It is suggested that these differences are, at least, partly related to the volume of sand contained in the bars; model predictions presented in the literature suggest that other geometric bar parameters, such as the water depth over the bar and in the bar trough, also play a role.

[31] The observed spatial and temporal crescentic bar behavior contrasts qualitatively with behavior predicted from the edge-wave template model and suggests that the

predictive skill of linear stability models should be reduced to the identification of the physical processes and conditions that might lead to crescentic bar development. Furthermore, there is not a consistent method for comparing predictions to observations because, in contrast to model assumptions, natural conditions are changing rapidly and the initial morphological configuration is already significantly perturbed. Nonlinear self-organization models are potentially better suited for a comparison against our field observations but require more realistic hydrodynamic and sediment transport descriptions before such a comparison can be carried out in a quantitative way.

[32] **Acknowledgments.** IMJvE was funded by the EU projects HUMOR and CoastView under contracts EVK3-CT-2000-00037 and EVK3-CT-2001-0054, respectively. GC was supported by the Office of Naval Research, Andrew W. Mellon Foundation and (New Zealand) Foundation for Research, Science and Technology. Also, we wish to thank (for various reasons) B. T. Werner, Doug Anderson, Koos Doekes, Isabelle Grujard, Stefan Aarninkhof, Bas van Dam, Irv Elshoff, John Stanley, Aart Kroon, and the Gold Coast City Council.

## References

- Aagaard, T. (1988), Nearshore bar morphology on the low-energy coast of northern Zealand, Denmark, *Geogr. Ann.*, *70A*, 59–67.
- Aagaard, T. (1989), Rhythmic beach and nearshore topography: Examples from Denmark, *Geogr. Tidsskr.*, *88*, 55–60.
- Aarninkhof, S. G. J., and R. A. Holman (1999), Monitoring the nearshore with video, *Backscatter*, *10*, 8–11.
- Allen, J. R., and N. P. Psuty (1987), Morphodynamics of a single-barred beach with a rip channel, Fire Island, NY, in *Proceedings of Coastal Sediments '87*, pp. 1964–1975, Am. Soc. of Civ. Eng., New York.
- Arbey, F. (1959), Observations nouvelles sur les croissants et sinuosités de plage, *C. R. Hebd. Seances de Acad. Sci.*, *248*, 3187–3189.
- Barousseau, J. P., and B. Saint-Guily (1981), Disposition, caractères et formation des barres d'avant-côte festonnées du Golfe du Lion, *Oceanol. Acta*, *4*, 297–304.
- Blondeaux, P. (2001), Mechanics of coastal forms, *Annu. Rev. Fluid Mech.*, *33*, 339–370.
- Bowen, A. J. (1997), Patterns in the water: Patterns in the sand?, in *Proceedings of Coastal Dynamics '97*, pp. 1–10, Am. Soc. of Civ. Eng., New York.
- Bowen, A. J., and D. L. Inman (1971), Edge waves and crescentic bars, *J. Geophys. Res.*, *76*, 8662–8671.
- Bowman, D., and V. Goldsmith (1983), Bar morphology of dissipative beaches: An empirical model, *Mar. Geol.*, *51*, 15–33.
- Brun, P. (1954), Migrating sand waves or sand humps, with special reference to investigations carried out on the Danish North Sea Coast, in *Proceedings of the 5th International Conference on Coastal Engineering*, pp. 269–295, Am. Soc. of Civ. Eng., New York.
- Bryan, K. R., and A. J. Bowen (1996), Edge wave trapping and amplification on barred beaches, *J. Geophys. Res.*, *101*, 6543–6552.
- Bryan, K. R., and A. J. Bowen (1997), Can bar-trapped edge waves cause bar formation, bar movement or bar growth?, in *Pacific Coasts and Ports '97 Conference*, pp. 1037–1042, Cent. for Adv. Eng., Univ. of Canterbury, Christchurch.
- Caballeria, M., G. Coco, A. Falques, and D. A. Huntley (2002), Self-organization mechanisms for the formation of nearshore crescentic and transverse bars, *J. Fluid Mech.*, *465*, 379–410.
- Caballeria, M., D. Calvete, G. Coco, N. Dodd, and A. Falques (2003a), Formation and alongshore spacing of crescentic bars, in *Proceedings of the 3rd Symposium on River, Coastal and Estuarine Morphodynamics [CD-ROM]*, Int. Assoc. for Hydraul. Res., Delft.
- Caballeria, M., G. Coco, and A. Falques (2003b), Crescentic patterns and self-organization processes on barred beaches, in *Proceedings of Coastal Sediments '03 [CD-ROM]*, Am. Soc. of Civ. Eng., New York.
- Calvete, D., and H. E. de Swart (2003), A nonlinear model study on the long-term behavior of shore face-connected sand ridges, *J. Geophys. Res.*, *108*(C5), 3169, doi:10.1029/2001JC001091.
- Calvete, D., N. Dodd, and A. Falques (2002), Morphological development of nearshore bedforms, in *Proceedings of the 28th International Conference on Coastal Engineering*, pp. 3321–3332, Am. Soc. of Civ. Eng., New York.

- Carter, R. W. G., and K. J. Kitcher (1979), The geomorphology of offshore sand bars on the north coast of Ireland, in *Proc. R. Irish Acad.*, 79, pp. 43–61.
- Castelle, B., F. Saint-Cast, and P. Bonneton (2003), 2DH modelling of sediment transport over a high energy barred-beach, in *Proceedings of Coastal Dynamics '03* [CD-ROM], Am. Soc. of Civ. Eng., New York.
- Chen, Y., and R. Guza (1998), Resonant scattering of edge waves by longshore periodic topography, *J. Fluid Mech.*, 369, 91–123.
- Christensen, E., R. Deigaard, and J. Fredsøe (1994), Sea bed stability on a long straight coast, in *Proceedings of the 24th International Conference on Coastal Engineering*, pp. 1865–1879, Am. Soc. of Civ. Eng., New York.
- Clos-Arceuduc, A. (1962a), Étude sur les vues aériennes des alluvions littorales d'allure périodique cordons littoraux et festons, *Bull. Soc. Fr. Photograph.*, 4, 13–21.
- Clos-Arceuduc, A. (1962b), Effects de la reflexion sur un obstacle d'une houle de longueur d'onde  $\lambda$ , *Photo Interprétation*, 1, 10.
- Coco, G., B. T. Werner, A. Falques, and M. Caballeria (2000), Comparison of two models for crescentic sand bars, in *Eos Trans. AGU*, 80(46), Fall Meet. Suppl., F672.
- Coco, G., M. Caballeria, A. Falques, and D. A. Huntley (2002), Crescentic bars and nearshore self-organization processes, in *Proceedings of the 28th International Conference on Coastal Engineering*, pp. 3765–3777, Am. Soc. of Civ. Eng., New York.
- Cowell, P. J., and B. G. Thom (1994), Morphodynamics of coastal evolution, in *Coastal Evolution: Late Quarternary Shoreline Morphodynamics*, edited by R. W. G. Carter and C. D. Woodroffe, pp. 33–86, Cambridge Univ. Press, New York.
- Damgaard, J., N. Dodd, L. Hall, and T. Chesher (2002), Morphodynamic modeling of rip channel growth, *Coastal Eng.*, 43, 199–221.
- De Boer, D. H. (1992), Hierarchies and spatial scale in process geomorphology: A review, *Geomorphology*, 4, 303–318.
- Deigaard, R., N. Drønen, J. Fredsøe, J. Hjelmeager Jensen, and M. P. Jørgensen (1999), A morphological stability analysis for a long straight barred coast, *Coastal Eng.*, 36, 171–195.
- Dolan, R., L. Vincent, and B. Hayden (1974), Crescentic coastal landforms, *Z. Geomorphol.*, 18, 1–12.
- Falqués, A., G. Coco, and D. Huntley (2000), A mechanism for the generation of wave-driven rhythmic patterns in the surf zone, *J. Geophys. Res.*, 105, 24,071–24,088.
- Froidefond, J. M., J. M. Gallissaires, and R. Prud'Homme (1990), Spatial variation in sinusoidal wave energy on a crescentic nearshore bar: Application to the Cap-Ferret coast, France, *J. Coastal Res.*, 6, 927–942.
- Furmanczyk, K., S. Musielak, J. Dudzinska, and I. Szakowski (2002), Bar systems as an indicator of circulation patterns in the Pomeranian bay, in *Proceedings of Littoral 2002*, pp. 305–309, Eurocoast/EUCC, Porto.
- Goldsmith, V., D. Bowman, and K. Kiley (1982), Sequential stage development of crescentic bars: HaHoterim Beach, southeastern Mediterranean, *J. Sediment. Petrol.*, 52, 233–249.
- Gourlay, M. R. (1968), Beach and dune erosion tests, *Rep. m935/m936*, Delft Hydraul. Lab., Delft.
- Greenwood, B., and R. G. D. Davidson-Arnott (1975), Marine bars and nearshore sedimentary processes, Kouchibouguac Bay, New Brunswick, Canada, in *Nearshore Sediment Dynamics and Sedimentation*, vol. 16, edited by J. Hails and A. Carr, pp. 123–150, John Wiley, Hoboken, N. J.
- Guza, R. T., and E. B. Thornton (1982), Swash oscillations on a natural beach, *J. Geophys. Res.*, 87, 483–491.
- Hino, M. (1974), Theory formation of rip-current and cuspidal forms, in *Proceedings of the 14th International Conference on Coastal Engineering*, pp. 901–919, Am. Soc. of Civ. Eng., New York.
- Holland, K. T., and R. A. Holman (1999), Wavenumber-frequency structure of infragravity swash motions, *J. Geophys. Res.*, 104, 13,479–13,488.
- Holman, R. A. (2000), Pattern formation in the nearshore, in *River, Coastal and Estuarine Morphodynamics*, edited by G. Seminara and P. Blondeaux, pp. 141–162, Springer-Verlag, New York.
- Holman, R. A., and A. J. Bowen (1982), Bars, bumps and holes: Models for the generation of complex beach topography, *J. Geophys. Res.*, 87, 457–468.
- Holman, R. A., and A. H. Sallenger (1985), Setup and swash on a natural beach, *J. Geophys. Res.*, 90, 945–953.
- Holman, R. A., and A. H. Sallenger (1993), Sand bar generation: A discussion of the Duck experiment series, *J. Coastal Res.*, SI 15, 76–92.
- Homma, M., and C. Sonu (1962), Rhythmic pattern of longshore bars related to sediment characteristics, in *Proceedings of the 8th International Conference on Coastal Engineering*, pp. 248–278, Am. Soc. of Civ. Eng., New York.
- Howd, P. A., and W. A. Birkemeier (1987), Storm-induced morphology changes during Duck85, in *Proceedings of Coastal Sediments '87*, pp. 834–847, Am. Soc. of Civ. Eng., New York.
- Huntley, D. A. (1980), Edge waves in a crescentic bar system, in *The Coastline of Canada*, pp. 111–121, Geol. Surv. of Can., Ottawa, Ont.
- Inman, D. L., and R. T. Guza (1982), The origin of swash cusps on beaches, *Mar. Geol.*, 49, 133–148.
- King, C. A. M., and W. W. Williams (1949), The formation and movement of sand bars by wave action, *Geogr. J.*, 113, 69–85.
- Klein, M. D., H. Schuttelaars, and M. J. F. Stive (2002), Linear stability of a double-barred coast, in *Proceedings of the 28th International Conference on Coastal Engineering*, pp. 3396–3408, Am. Soc. of Civ. Eng., New York.
- Komar, P. D. (1998), *Beach Processes and Sedimentation*, Prentice-Hall, Old Tappan, N. J.
- Lippmann, T. C., and R. A. Holman (1989), Quantification of sand bar morphology: A video technique based on wave dissipation, *J. Geophys. Res.*, 94, 995–1011.
- Lippmann, T. C., and R. A. Holman (1990), The spatial and temporal variability of sand bar morphology, *J. Geophys. Res.*, 95, 11,575–11,590.
- MacMahan, J., A. J. H. M. Reniers, E. B. Thornton, T. Stanton, and R. G. Dean (2002), RIPEX: Rip current pulsation measurements, in *Proceedings of the 28th International Conference on Coastal Engineering*, pp. 736–746, Am. Soc. of Civ. Eng., New York.
- Murray, A. B. (2003), Contrasting the goals, strategies, and predictions associated with simplified numerical models and detailed simulations, in *Prediction in Geomorphology*, *Geophys. Monogr. Ser.*, vol. 135, edited by P. R. Wilcock and R. M. Iverson, pp. 151–165, AGU, Washington, D. C.
- Nafaa, M. G., and O. E. Frihy (1993), Beach and nearshore features along the dissipative coastline of the Nile Delta, Egypt, *J. Coastal Res.*, 9, 423–433.
- Phillips, J. D. (1999), *Earth Surface Systems—Complexity, Order and Scale*, Blackwell, Malden, Mass.
- Plant, N. G., R. A. Holman, M. H. Freilich, and W. A. Birkemeier (1999), A simple model for interannual sandbar behavior, *J. Geophys. Res.*, 104, 15,755–15,776.
- Plant, N. G., K. T. Holland, and J. A. Puleo (2002), Analysis of the scale of errors in nearshore bathymetric data, *Mar. Geol.*, 191, 71–86.
- Reniers, A. J. H. M., J. A. Roelvink, and E. B. Thornton (2004), Morphodynamic modeling of an embayed beach under wave group forcing, *J. Geophys. Res.*, 109, C01030, doi:10.1029/2002JC001586.
- Rivière, A., F. Arbey, and S. Verhét (1961), Remarque sur l'évolution et l'origine des structures de plage à caractère périodique, *C. R. Hebd. Seances Acad. Sci.*, 252, 767–769.
- Ruessink, B. G. (1992), The nearshore morphology of Terschelling (1965–1991), *Rep. R92-II*, Inst. for Mar. and Atmos. Res., Utrecht.
- Ruessink, B. G., M. G. Kleinhans, and P. G. L. Van den Beukel (1998), Observations of swash under highly dissipative conditions, *J. Geophys. Res.*, 103, 3111–3118.
- Ruessink, B. G., I. M. J. Van Enckevort, K. S. Kingston, and M. A. Davidson (2000), Analysis of observed two- and three-dimensional nearshore bar behaviour, *Mar. Geol.*, 169, 161–183.
- Sallenger, A. H., R. A. Holman, and W. Birkemeier (1985), Storm-induced response of a nearshore-bar system, *Mar. Geol.*, 64, 237–257.
- Shand, R. D., D. G. Bailey, and M. J. Shepherd (2001), Longshore realignment of shore-parallel sand-bars at Wanganui, New Zealand, *Mar. Geol.*, 179, 147–161.
- Shepard, F. P. (1952), Revised nomenclature for depositional coastal features, *Bull. Am. Assoc. Petrol. Geol.*, 36, 1902–1912.
- Short, A. D. (1979), Three dimensional beach-stage model, *J. Geol.*, 87, 553–571.
- Short, A. D., and T. Aagaard (1993), Single and multi-bar beach change models, *J. Coastal Res.*, SI 15, 141–157.
- Sonu, C. J. (1968), Collective movement of sediment in littoral environment, in *Proceedings of the 11th International Conference on Coastal Engineering*, pp. 373–400, Am. Soc. of Civ. Eng., New York.
- Sonu, C. J. (1973), Three-dimensional beach changes, *J. Geol.*, 81, 42–64.
- Stewart, C. J., and R. G. D. Davidson-Arnott (1988), Morphology, formation and migration of longshore sandwaves; Long Point, Lake Erie, Canada, *Mar. Geol.*, 81, 63–77.
- Suzuki, K., S. Takahashi, N. Yamagata, O. Horita, Y. Kuriyama, S. Aaminkhof, G. Ruessink, and I. Elshoff (2002), Field observations of Miyazaki beach using argus video technique (in Japanese), *Proc. Coastal Eng. Jpn.*, 47, 571–575.

- Thornton, E. B., and R. T. Guza (1982), Energy saturation and phase speeds measured on a natural beach, *J. Geophys. Res.*, *87*, 9499–9508.
- Turner, I. L., V. M. Leyden, G. Symonds, J. McGrath, A. Jackson, T. Jancar, S. G. J. Aarninkhof, and I. E. Elshoff (2000), Predicted and observed coastline changes at the Gold Coast artificial reef, in *Proceedings of the 27th International Conference on Coastal Engineering*, pp. 1836–1847, Am. Soc. of Civ. Eng., New York.
- Van Enckevort, I. M. J., and B. G. Ruessink (2001), Effects of hydrodynamics and bathymetry on video estimates of nearshore sandbar position, *J. Geophys. Res.*, *106*, 16,969–16,979.
- Van Enckevort, I. M. J., and B. G. Ruessink (2003), Video observations of nearshore bar behaviour. part 2: Alongshore non-uniform variability, *Cont. Shelf Res.*, *23*, 513–532.
- Vittori, G., H. De Swart, and P. Blondeaux (1999), Crescentic bedforms in the nearshore region, *J. Fluid Mech.*, *381*, 271–303.
- Wijnberg, K. M. (1995), Morphologic behaviour of a barred coast over a period of decades, Ph.D. thesis, Dept. of Phys. Geogr., Utrecht Univ., Utrecht.
- Wijnberg, K. M., and F. C. J. Wolf (1994), Three-dimensional behaviour of a multiple bar system, in *Proceedings of Coastal Dynamics '94*, pp. 59–73, Am. Soc. of Civ. Eng., New York.
- Woodroffe, C. D. (2003), *Coasts: Form, Process and Evolution*, Cambridge Univ. Press, New York.
- Wright, L. D., and A. D. Short (1984), Morphodynamic variability of surf zones and beaches: A synthesis, *Mar. Geol.*, *56*, 93–118.
- Wright, L. D., P. Nielsen, N. C. Shi, and A. D. Short (1986), Morphodynamics of a bar-trough surf zone, *Mar. Geol.*, *70*, 251–285.
- 
- G. Coco, National Institute of Water and Atmospheric Research, P.O. Box 11-115, Hamilton, New Zealand. (g.coco@niwa.co.nz)
- R. A. Holman, Coastal Imaging Laboratory, College of Oceanic and Atmospheric Sciences, Oregon State University, Corvallis, OR 97331-5503, USA. (holman@coas.oregonstate.edu)
- N. G. Plant, Naval Research Laboratory, Stennis Space Center, MS 39529, USA. (nplant@nrlssc.navy.mil)
- B. G. Ruessink and I. M. J. van Enckevort, Institute for Marine and Atmospheric Research, Department of Physical Geography, Utrecht University, P.O. Box 80.115, N-3508 TC Utrecht, Netherlands. (g.ruessink@geog.uu.nl; i.vanenckevort@geog.uu.nl)
- K. Suzuki, Marine Environment and Engineering Department, Port and Airport Research Institute, Nagase 3-1-1, Yokosuka, Kanagawa 239-0826, Japan. (suzuki\_k@pari.go.jp)
- I. L. Turner, School of Civil and Environmental Engineering, University of New South Wales UNSW, Sydney, NSW 2052, Australia. (ian.turner@unsw.edu.au)